HiLL PUBLISHING

Engineering Advances, 2022, 2(1), 128-140
https://www.hillpublisher.com/journals/ea/
ISSN Online: 2768-7961

Numerical Investigation of Adiabatic Film Cooling Effectiveness over Flat Plate with Barchan Dune Shape Ramp Configuration

Grine Mustapha[1,*], Ben Ali Kouchih Fatima[2], Khadidja Boualem[2], Azzi Abbès[2]

[1]ELM Department, Institute of Maintenance and Industrial Safety, Oran 2 University, Oran, Algeria.
[2]Laboratoire Aero Hydrodynamique Navale, (LAHN) USTO-MB, Oran, Algeria.

How to cite this paper: Grine Mustapha, Ben Ali Kouchih Fatima, Khadidja Boualem, Azzi Abbès. (2022) Numerical Investigation of Adiabatic Film Cooling Effectiveness over Flat Plate with Barchan Dune Shape Ramp Configuration. *Engineering Advances*, 2(1), 128-140.
DOI: 10.26855/ea.2022.06.012

Received: April 15, 2022
Accepted: May 12, 2022
Published: June 24, 2022

***Corresponding author:** Grine Mustapha, ELM Department, Institute of Maintenance and Industrial Safety, Oran 2 University, Oran, Algeria.
Email: grine890@gmail.com

Abstract

In this study, the effect of low and high blowing ratios on film cooling efficiency over a flat plate with Barchan Dune Shape Ramp is presented. The blowing ratios considered in this paper are, M=0.25, 0.5, 0.85, 1.0 and 1.5. The concept of the Barchan Dune Shape Ramp (BDSR) can generate anti-counter rotating vortices (anti-CRV) that's help in the distribution of coolant flow. The BDSR located upstream of the injection hole. All cases are simulated using the commercial software ANSYS CFX 16. The k-ε RNG is utilized as a closure model for the averaged Navier Stokes equations. The validation of current calculations is made by comparison with experimental data found in the literature. The main result of this study reveals that the use of BDSR is limited for blowing ratios less than one.

Keywords

Film Cooling efficiency, BDSR, Anti CRV

1. Introduction

In the gas turbine industry, the efficiency and the power of the machines are proportional to the highest temperature of the cycle. This temperature corresponds to that of the combustion gases which directly attack the blades of the first stages of the gas turbine, hence the obligation to adopt sophisticated and well-studied cooling processes [1]. Film cooling is probably the most efficient blade-cooling mechanism employed in gas-turbine technology. The cooling performance can be affected by several parameters, the blade geometry, blowing ratio, the inclination angle of the jet, free stream turbulence, etc.

Several investigations were conducted to understand the complex mechanisms of the film cooling process, among them [2-4], in studies, many geometrical configurations were presented, leading-edge turbine blades and cool ant holes on a flat plate; this latter is considered as the conventional and the most used.

Most of the techniques that were used to enhance the film cooling performance concentrate on the hole geometry to modify the boundary-layer/cooling jet interactions. The compound angle is one of the methods that is presented by Schmidt et al. [5], their results indicated that the much-improved lateral distribution of coolant had provided by the compound angle holes with expanded exits at all blowing ratios. Ligrani et al. [6-7] found that the compound angle injection can improve significantly the film cooling effectiveness compared to a simple angled hole. The jets installed in trenches were used by [8-9] to improve film cooling effectiveness. Kebir and Azzi [10] presented two different designs of cooling holes, a hole situated on the crest of the wave and a hole through wave. Their results indicate that the crest position of the cooling hole is more efficient than the trough position. Ben Ali Kouchih et al. [11] tested backward injection holes with Barchan-dune-shaped shells in improving film cooling performance. Gritsch et al. [12-13] tested

three-hole geometries, simple angle cylindrical holes, fan-shaped holes and laidback fan shaped. They showed that laidback fan-shaped holes provide higher laterally averaged film cooling effectiveness compared to other shaped holes.

To eliminate or reduce the size of counter rotating vortices (CRV), Chang et al. [14] have used combined-hole. They showed that this configuration can reduce the formation of kidney vortices that are harmful to film cooling. Hassan et al. [15] have combined two cylindrical holes as a unit to improve the film cooling performance at all blowing ratios. A novel combined hole was presented by Wang et al. [16]. They noticed that the combined hole provides uniform film cooling performance in both downstream and lateral directions and reduced the aerodynamic loss.

In recent years, another method for cooling performance enhancement is to modify the flow behavior by placing an upstream ramp of a coolant hole. Zaman et al. [17] and Shinn and Vanka [18] have shown the effect of a micro-ramp placed behind the film hole. It has been found that this configuration generates antivortices that can eliminate the jet lifting off improving the film cooling effectiveness. Zhou and Hu [19, 20] tested a new ramp design inspired by the shape of sand dunes, (Barchan-dune-shaped). They noted that this new concept improves the film cooling efficiency and reduce adequately the kidney vortices.

The present study aims to analyze the flow structures over a flat plate using the BDSR concept to improve the film cooling performance. The presence of this configuration can definitely improve the film cooling performance by the generation of an anti-counter rotating vortices (anti-CRV) that's help in the distribution of coolant flow and cover the whole surface. The geometry was modified by adding the concept of ramp in the form of a Barchan-dune-shaped (BDS) upstream of the injection hole. Five blowing ratios are considered (0.25, 0.50, 0.85, 1.00, and 1.85) and one length-to-diameter ratio 1.75. To carry out this work, several simulations were conducted using ANSYS CFX 14.0 software [21]. By using the solver package, we define a high precision of distribution, the solution of the Reynolds Averaged Navier-Stokes equations (RANS) is obtained by using the finite volume method for the discretization of the continuity, momentum, and energy equations. Zhang and Hassan [22] compared the model RNG k-ε [23, 24, 25] with another model (Realizable k-ε Standard wall, Standard wall, Standard k- ε). The results obtained using this model are more consistent with the experimental data for the prediction of film cooling effectiveness than those obtained by other models. This model has been adopted in our work due to its ease of use for initial iterations, initial screening of alternative designs, and parametric studies. At the same time, it performs poorly for complex flows involving severe pressure gradient, separation, strong streamline curvature. The flow is considered as an incompressible perfect gas, the regime is stationary. The convergence criteria are obtained when all the residuals are 10^{-6}.

2. Flow geometry, grids and boundary conditions

Two configurations are considered in this study. The first is a cylindrical geometry based on the experimental work of Sinha et al. [26]. The second is the proposed new modification based on the concept of the shape ramp of the Barchan-dune-shaped (BDSR) upstream of the injection holes. Its maximum height and width are H=0.5D and W=2.85D respectively as is illustrated in Figure 1.

Figure 1 represents the geometry of the dune-shaped ramp while Figure 2 represents the domain of calculation appropriate to the simulation.

3. Computational domain and boundary conditions

3.1. Computational domain

A single row of cylindrical holes inclined of 35° in the direction of flow is considered for both cases. The lateral spacing of the holes is set to 3D, where D is the diameter of the hole, its value is 12.7 mm. One-hole length-to-diameter ratio of 1.75 is considered in this study. The range of calculation extends from the input plane up to 50D in the streamwise direction of flow and from the bottom of the flat plate to 20D in the vertical direction.

In the spanwise direction, the domain extends between two injection holes. The conditions of symmetry are imposed on the lateral planes. To improve the application of the velocity profile of the flux injected at the entrance of the hole injection, a plenum is introduced into the computational domain while the boundary layer has been fully developed.

3.2. Boundary conditions

The boundary conditions are defined in the CFX Pre model of the CFX14 calculation code. The flow velocity of the mainstream was set to U = 20 m/s, according to the experience of Sinha et al. [26]. A turbulence intensity of the free flow Tu = 5% and the relative pressure is equal to 0 bar at the outlet of the two flows (mainstream and secondary) and a dimensionless eddy viscosity of $\mu_t/\mu_\infty = 50$.

On the wall surface of the flat plate, the employed boundary conditions were no-slip boundary conditions for the velocity and the adiabatic state for the temperature. Similar conditions were applied to the pipe and plenum internal walls. Because the upper surface of the domain was set relatively far from the flat plate, the density ratios between the injection

flow and the main flows are kept as in the experimental configuration $\rho_{jet}/\rho_{\infty} = 1.2$. The working flow temperature is set to Air at 300°K for the main flow, and 250° K for the secondary jet flow. Five injection ratios of 0.25, 0.5, 0.85, 1.0 and 1.5 are considered.

4. Presentation of the BDSR case

As the base case, and keeping the same geometric parameters, we added a dune shape ramp in the new geometry. This dune is called dune Barchan, named after its inventor. This dune was placed upstream of the injection hole at a distance L from the center of the latter and with a height H as shown in Figure 1. The geometric configuration of the BDSR model used in this study was taken from the experimental study of Wenwu Zhou and Hui Hu [18].

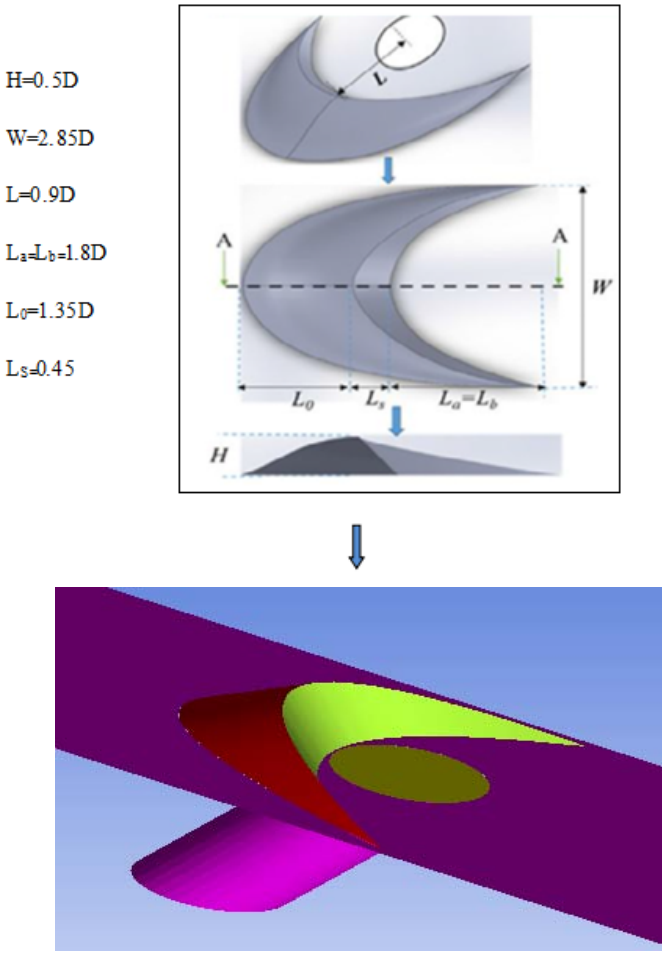

Figure 1. Schematic of the geometric configuration of the dune-shaped ramp (BDSR).

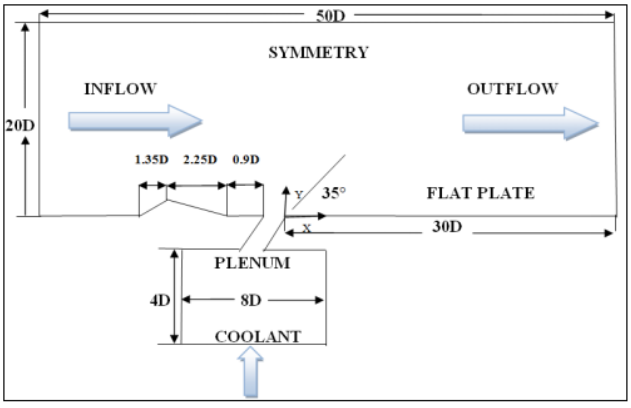

Figure 2. Computation domain and the boundary conditions.

5. Computational Grid

In this study, the meshing is performed for an injection ratio M = 0.5 for central adiabatic film cooling. Three meshing of about 1,000,000, 1,500,000 and 2,000,000 hexahedral elements were tested. The mesh of 1,000,000 hexahedral cells was adopted for our work because of its compatibility with the experimental study of Sinha et al. as shown in Figure 3. Refining the meshing is more pronounced near the walls and in the vicinity of the injection hole. The calculation grid is very refined in this region. The calculation grid was created using ICEM CFD 14.0. Figure 4 shows samples of zoomed regions of the computational grid in the vicinity of the injection hole for the proposed model (BDSR).

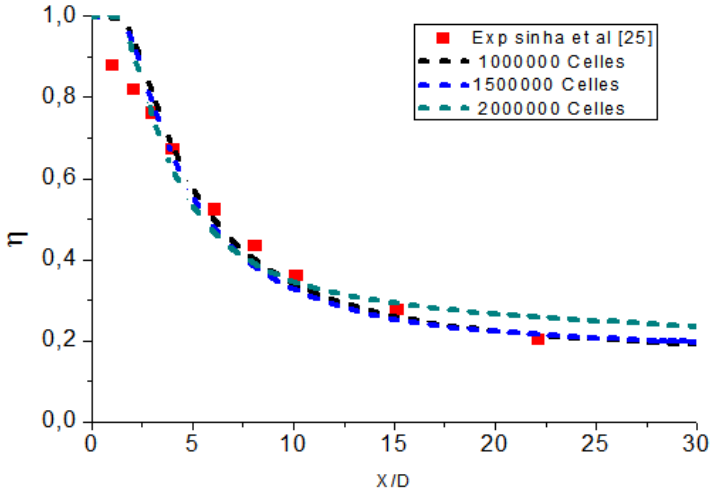

Figure 3. Sensitivity grid, Centerline adiabatic film cooling effectiveness for three different meshing.

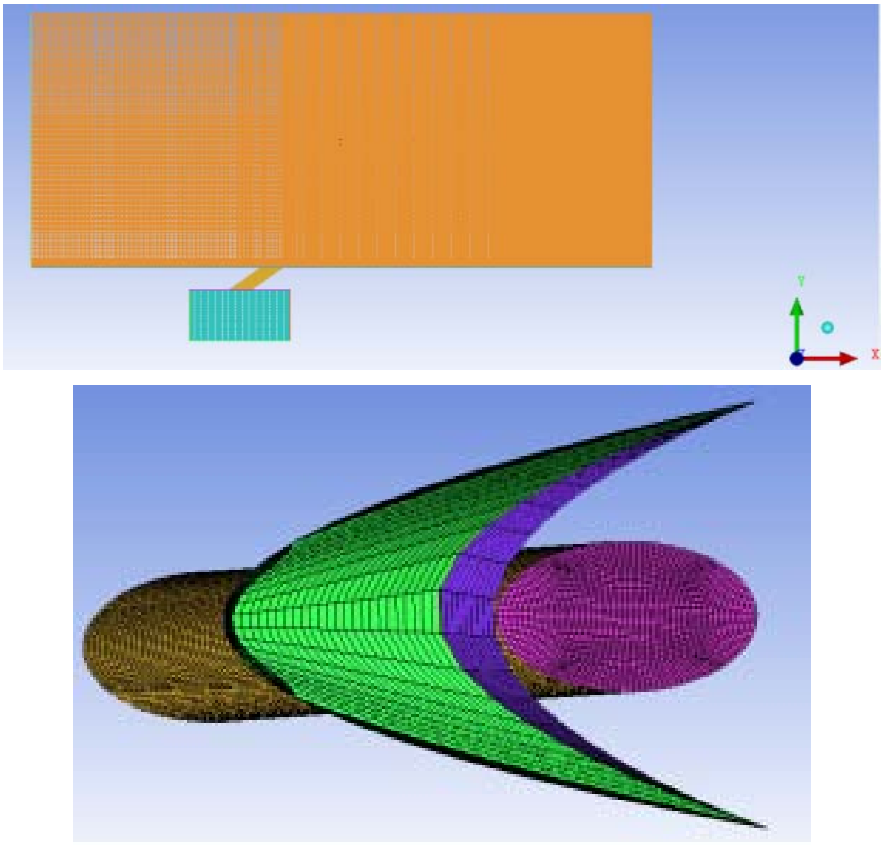

Figure 4. The calculation grid for the BDSR case.

6. Results and Discussion

6.1. Laterally averaged adiabatic film cooling effectiveness

In the first section, the discussion will be based on the so-called laterally averaged adiabatic film cooling effectiveness<η>, which is defined by:

$$< \eta > = \frac{1}{L}\int_L \eta dz \quad \text{Eqs.} \tag{1}$$

Where L represents the spanwise dimension of the plate and ηis the adiabatic film cooling effectiveness, defined by:

$$\eta = \frac{T_\infty - T}{T_\infty - T_c} \quad \text{Eqs.} \tag{2}$$

Where T_∞ and T_c, stand for the main flow and the jet temperature respectively. Adiabatic film cooling effectiveness is defined in such a way to be *1* for perfect cooling and *0* for no cooling at all, while averaged adiabatic film cooling effectiveness <η> is used to highlight the lateral spreading of the cold film over the blade.

Blowing ratio and hole length-to-diameter are the two parameters used in the present study. The blowing ratio (M) is defined by:

$$M = \frac{\rho_f U_f}{\rho_\infty U_\infty} \quad \text{Eqs.} \tag{3}$$

Where ρ_f and $\rho_\infty$are the jets and main flow densities, while U_f and U_∞ are the perpendicular velocities of jet and main flow respectively. In all present computations, the density ratio is fixed at *1.2*. As in Sinha's [22] experiment, U_∞ is fixed at 20m/s and U_f is computed according to the targeted blowing ratio. Boundary inlet velocity at plenum entry is computed according to the mass conservation law.

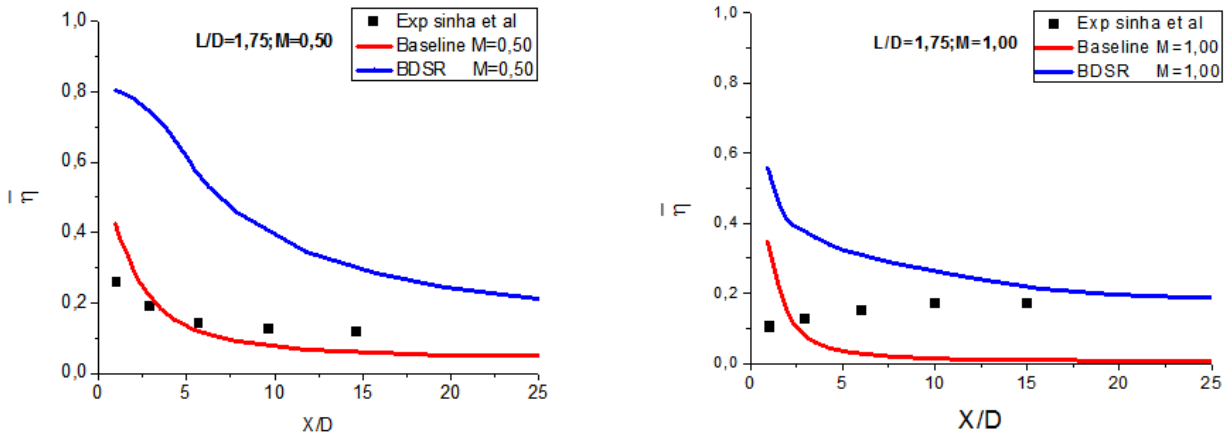

Figure 5. Laterally averaged adiabatic film cooling effectiveness M = 0.5; M = 1.0, L/D =1.75.

Figure 5 shows the evolution of laterally averaged adiabatic film cooling effectiveness of the case Baseline and BDSR configurations for injection ratios M= 0.5, M=1.0, L/D = 1.75 compared to available data from the experience of Sinha and et al. We can see that the values obtained with the Baseline configuration are close to the experimental data, whereas the pace is well captured. For this case, the detachment of the jet resulting in a decrease in laterally averaged adiabatic film cooling effectiveness occurs closer to the injection hole with the ratio M = 1.00 than with the ratio M = 0.50.On the other hand, the results of the laterally averaged adiabatic film cooling effectiveness obtained with the BDSR configuration are superior to the results obtained with the baseline configuration.

Table 1. The studied cases

Injection ratios	Base line case	BDSR case
M=0.25	B_M0.25_L175	BD_M0.25_L175
M=0.50	B_M0.50_L175	BD_M0.50_L175
M=0.85	B_M0.85_L175	BD_M0.85_L175
M=1.00	B_M1.00_L175	BD_M1.00_L175
M=1.50	B_M1.50_L175	BD_M1.50_L175

6.2. Centerline adiabatic film cooling effectiveness:

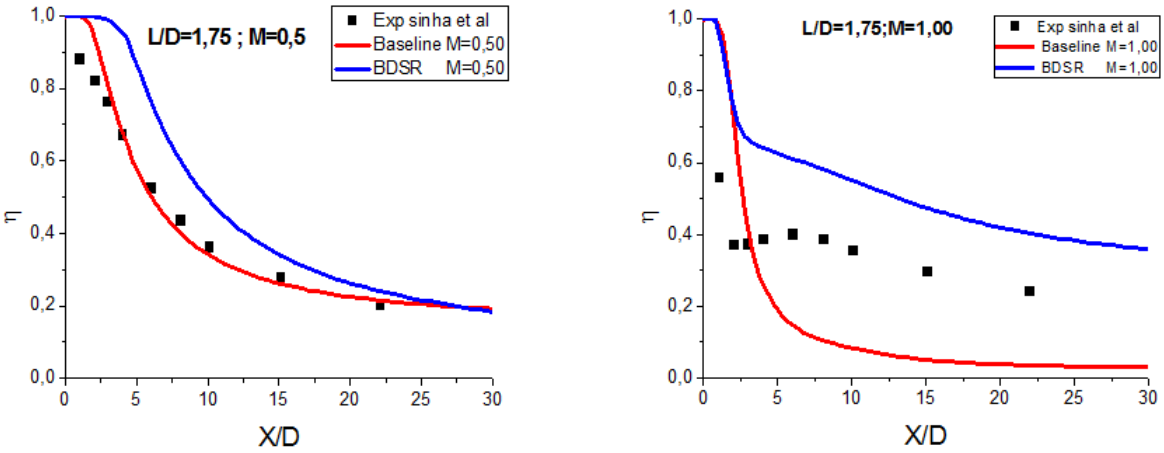

Figure 6. Centerline adiabatic film cooling effectiveness M = 0.5; M = 1.0, L/D = 1.75.

Figure 6 represents the Centerline adiabatic film cooling effectiveness for the injection ratios M = 0.5 and M = 1.0 with L/D ratio = 1.75. We note a good concordance of the results obtained with the experimental results of Sinha et al. [26].

For the M= 0.50 ratio, we observe that the jet remains attached to the wall and then the laterally averaged adiabatic film cooling effectiveness decreases monotonically in the streamwise direction. We also note that the case of BDSR gives a better prediction in the region X/D >2.5 D.

For the M= 1.00 ratio, we observe that the case of BDSR gives a better efficiency compared to the case of Baseline from X/D >5D.

Comparing the results of the two Figures 5 and 6, we find that generally, when the centerline film-cooling effectiveness is higher, this corresponds to a lateral spreading that is being too weak. So, a higher centerline film cooling effectiveness corresponds to a lower<η>. This phenomenon is due to a weak lateral diffusion.

6.3. Comparison of injection ratios of centerline film cooling effectiveness and the laterally averaged adiabatic film cooling effectiveness for two configurations:

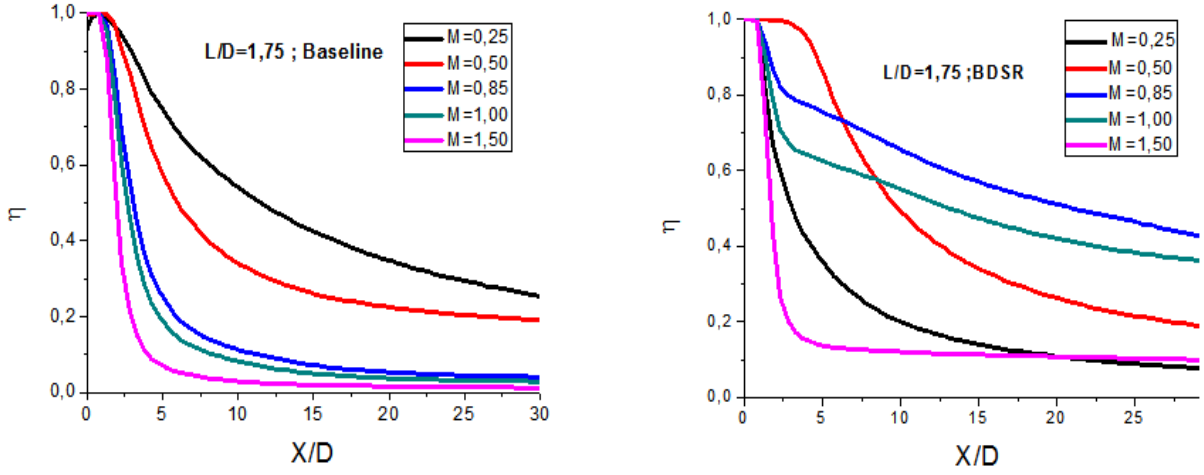

Figure 7. Centerline film-cooling effectiveness for different injection ratios M = 0.25, M = 0.5, M = 0.85, M = 1.0, M = 1.5, L/D = 1.75.

Figure 7 represents a comparison of the values of the centerline film-cooling effectiveness for different injection ratios (M = 0.25, M = 0.5, M = 0.85, M = 1.0 and M = 1.5) with diameter ratio L/D= 1.75 for the two configurations Baseline and BDSR.

One can see that in the case of Baseline, the centerline film-cooling effectiveness decreases while the injection ratio increases. This is explained by the phenomenon of attachment of the jet. For the BDSR case, the centerline film-cooling effectiveness records rising for the ratio from M = 0.25 to M = 0.85, the latter being a critical value. The centerline

film-cooling effectiveness starts to decrease after this value which is in agreement with the physical aspect related to the detachment of the jet, Therefore, we conclude that the injection rate M = 0.85 is the most favorable case. This allows us to distinguish two categories of injection ratios, Low injection ratios which are M = 0.25 and M = 0.50 and Higher injection ratios that are M = 0.85, M = 1.00 and M = 1.50.

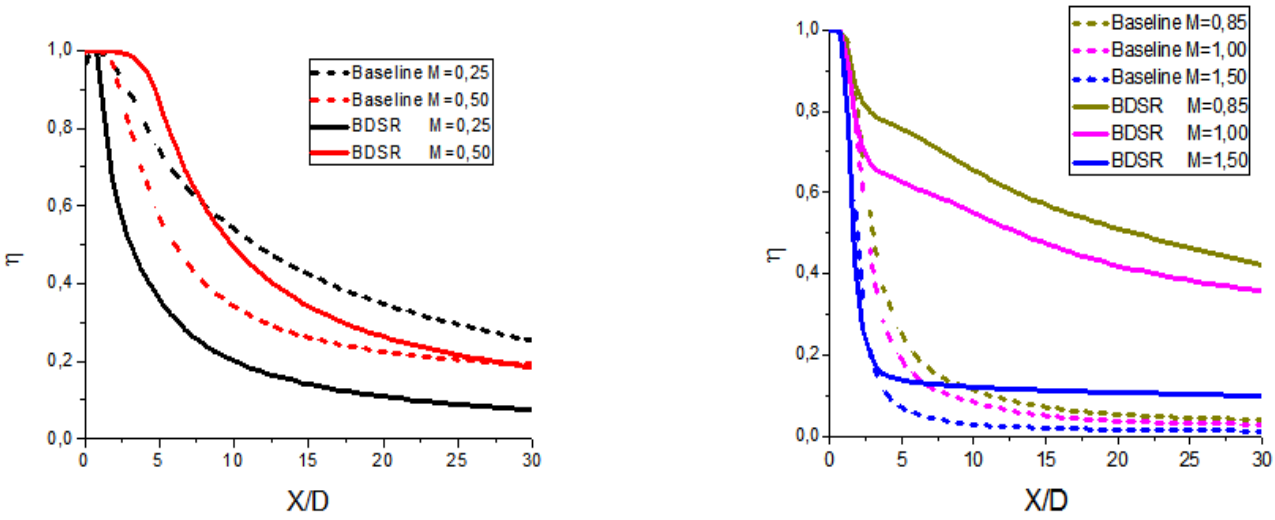

Figure 8. Centerline film-cooling effectiveness for low and higher injection ratios for the Baseline and BDSR cases.

For low injection ratios, the best ratio injection of the Baseline case is M = 0.25. Whereas for the BDSR case, the best ratio injection is M = 0.50. For the higher injection ratios, for two cases, the best ratio is M = 0.85, the centerline film-cooling effectiveness decreases with increasing ratios. However, the η is better with the case of BDSR than with the case of Baseline.

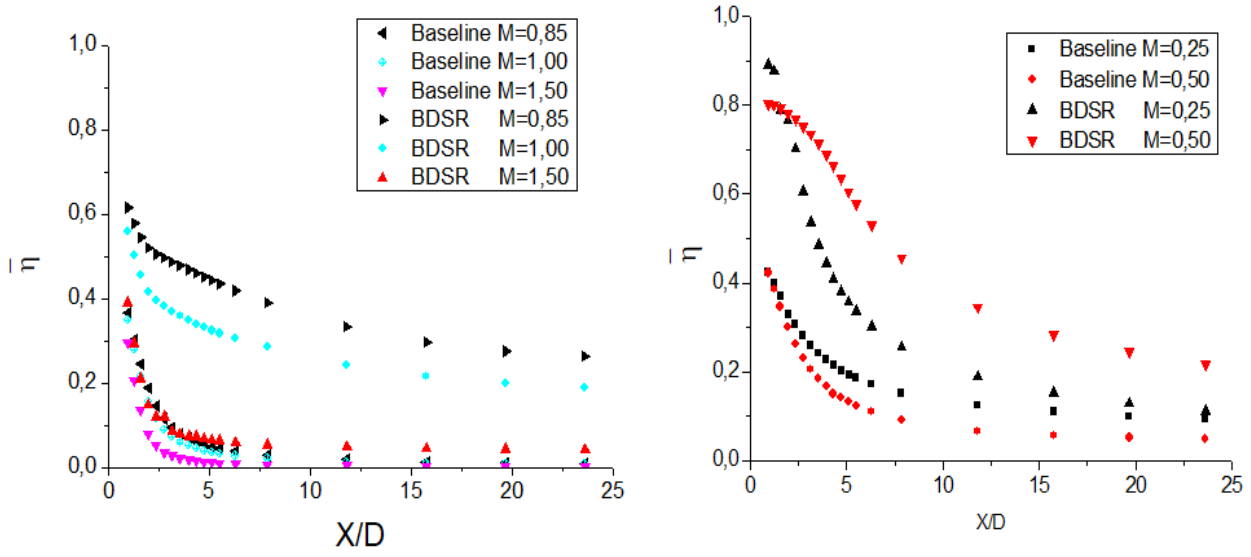

Figure 9. Laterally averaged adiabatic film cooling effectiveness for low and higher injection ratios M = 0.25, 0.5, 0.85, 1.0, 1.5.

Figure 9 shows laterally averaged adiabatic film cooling effectiveness for low and higher injection ratios of the Baseline and BDSR cases.

It can be clearly seen that the laterally averaged adiabatic film cooling effectiveness for low ratios monotonically decreases in the direction of flow. This is explained by the fact that the jet remains attached to the wall. For low injection ratios, the case of BDSR is better compared to the case of Baseline for all injection ratios. For the higher injection ratios, in the two cases, the best ratio is M = 0.85, effectiveness decreases with increasing ratios. However, effectiveness is better with the case of BDSR than with the case of Baseline. This performance can be explained by the good propagation of the cooling film on the flat plane and this is due to the location of the BDSR upstream of the injection hole.

6.4. Distributions of the spanwise film-cooling effectiveness:

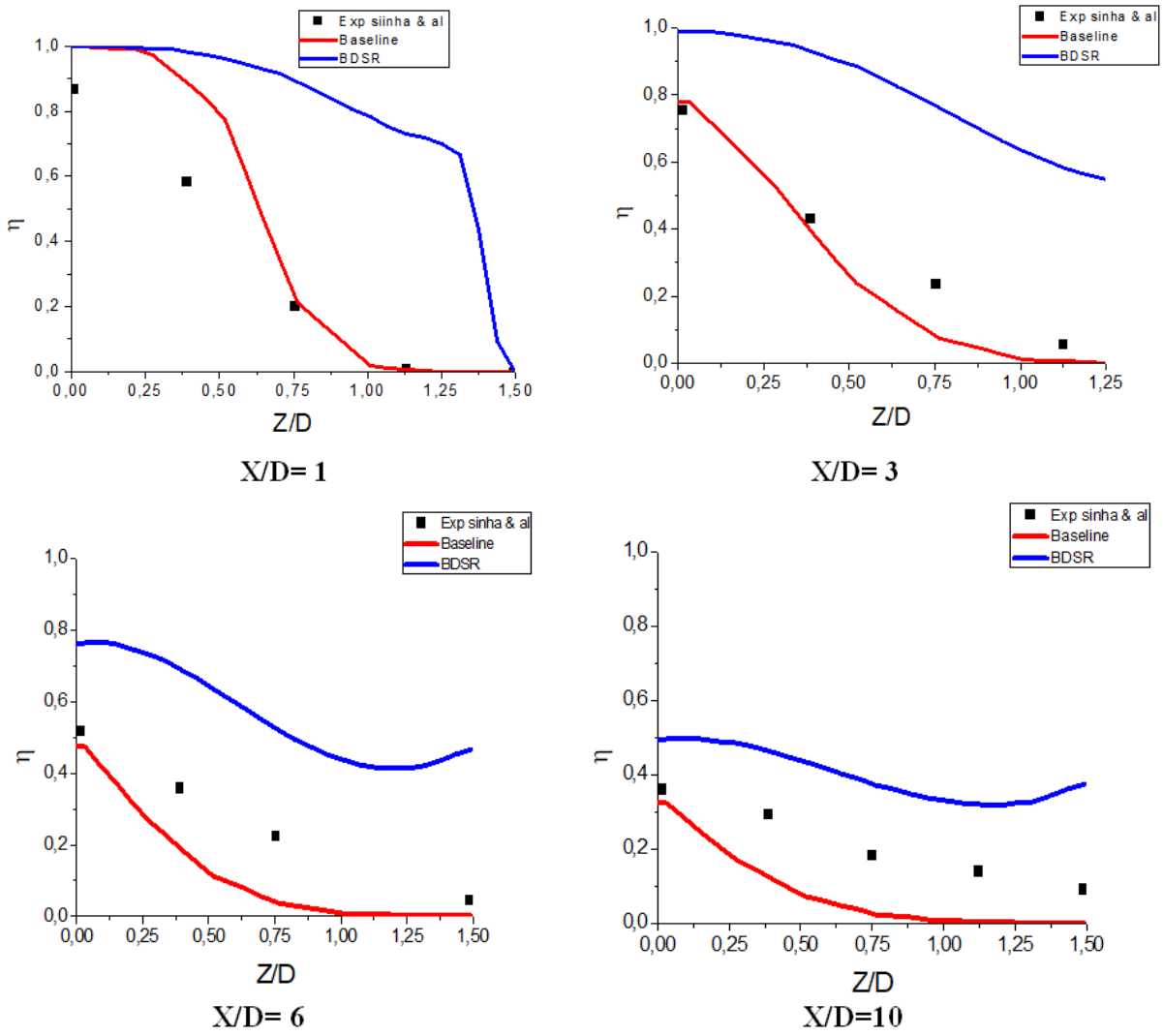

Figure 10. Distributions of the spanwise film-cooling effectiveness for M=0.5 at four cross-flow locations.

Figure 10 shows the distributions of the spanwise film-cooling effectiveness for M=0.5 at four cross-flow locations. The jet spreading over the wall is analyzed by examining the spanwise distributions of *h* on the channel surface plotted in Fig.12 at X/D=1, 3, 6, and 10. It shows that η obtained with the case of BDSR is better compared with that obtained with the case of Baseline at the exit of the injection hole. We notice for all spanwise that there is a good concordance with the experimental of Sinha et al. [26]. For the case of BDSR, we note that η is higher than that of Baseline when X/D= 3, X/D=6 and X/D=10. This can be explained by the geometry of the concept of the ramp in the form of dune that plays the role of an obstacle for the hot flow.

6.5. Adiabatic Film Cooling Effectiveness on the plate flat for Different Injection Ratios

M=0.25

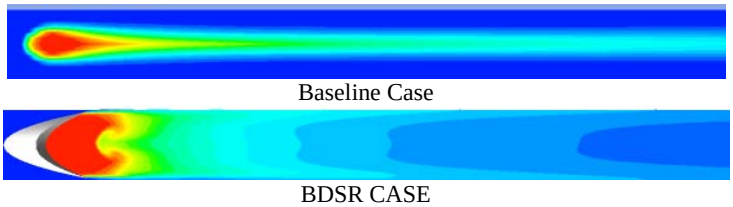

Baseline Case

BDSR CASE

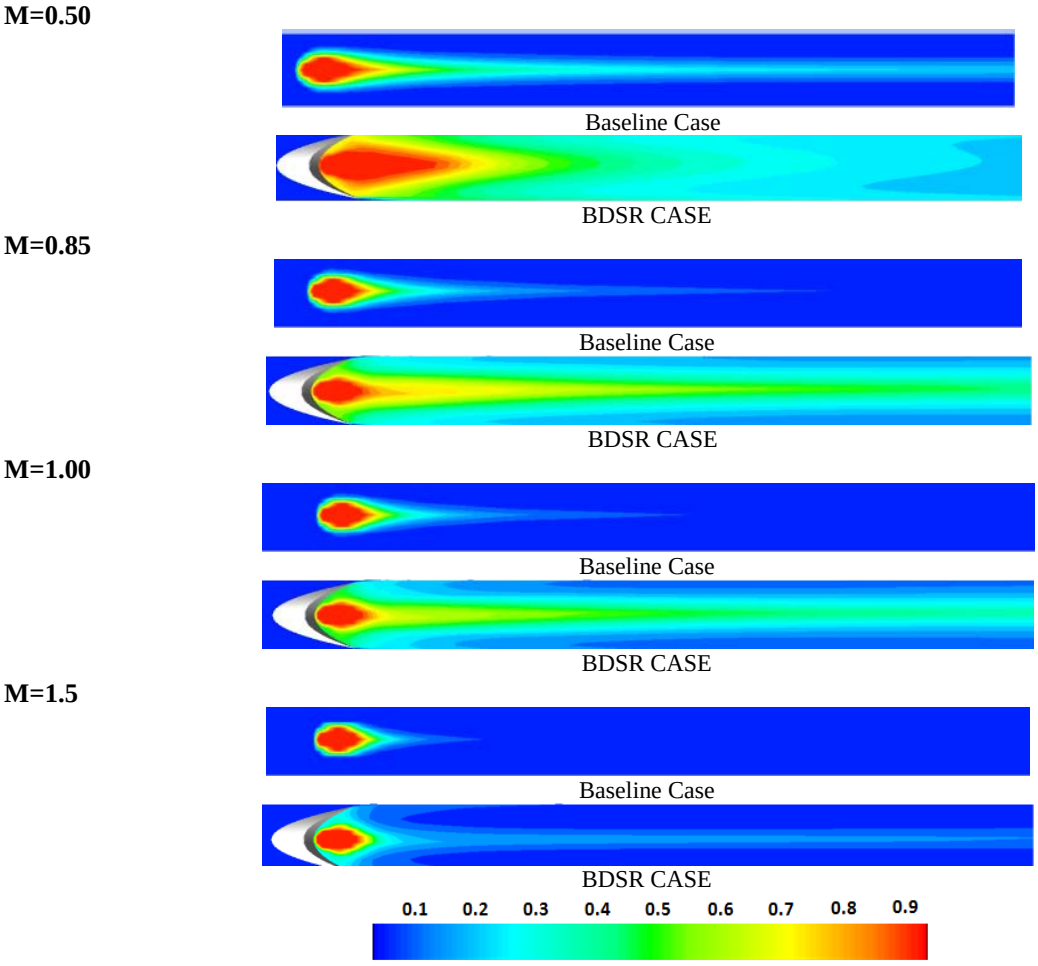

Figure 11. 4 Adiabatic Film Cooling Effectiveness on the plate flat for Different Injection Ratios M = 0.25, M = 0.5, M = 0.85, M = 1.0, M = 1.5.

Figure 11 shows a comparison of the adiabatic film cooling effectiveness of the flat plate for two configurations at different injection ratios (higher and low).

For low injection ratios, the case of Baseline shows that the jet remains attached to the hole, the space between the injection holes is less well protected than in the case of BDSR. The adiabatic film cooling effectiveness in the case of BDSR is always better than that of the case of the Baseline. In the case of BDSR, the area covered by the film cooling is almost double that of the Baseline. In the case of BDSR, for injection ratios M = 0.25 to M = 0.85, we notice that the coverage of the film cooling improves in the lateral sense of the jet. For M = 0.85, the protected surface of the plate begins to reduce. These discussions are agreed with the results obtained previously in Figures 8 and 9.

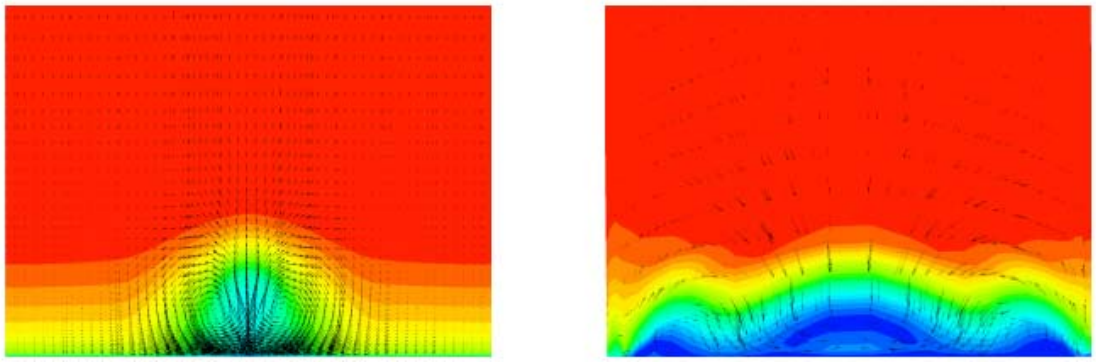

M=0.5

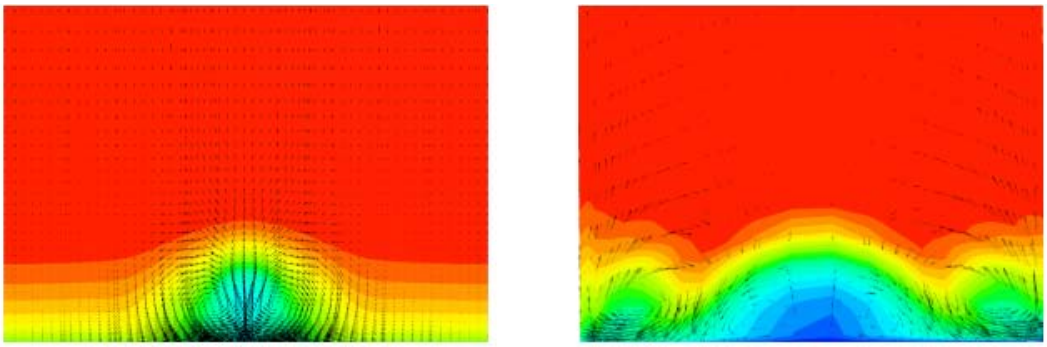

BASELINE CASE BDSR CASE

M=0.85

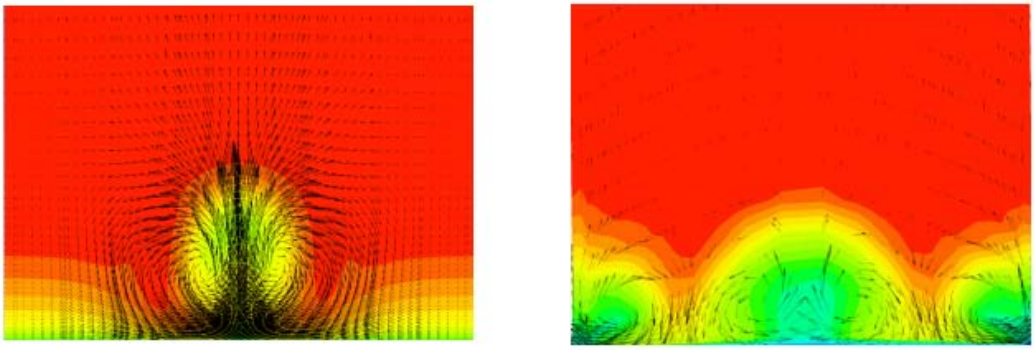

BASELINE CASE BDSR CASE

M=1

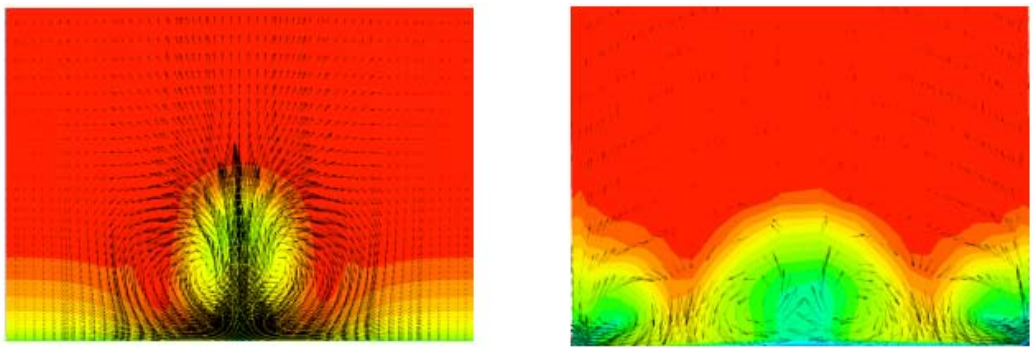

BASELINE CASE BDSR CASE

M=1.5

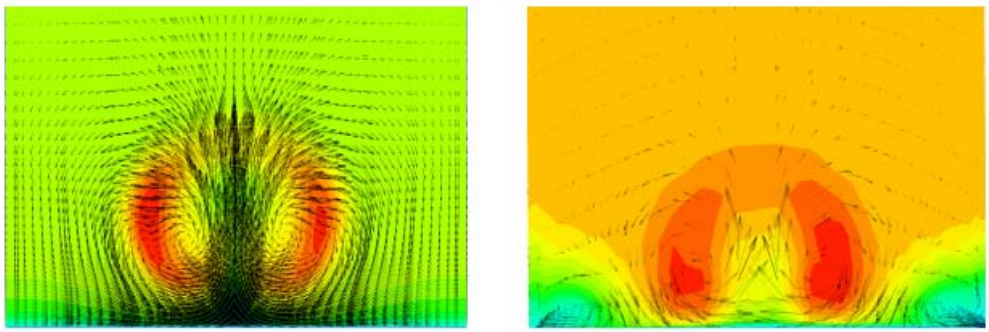

BASELINE CASE BDSR CASE

Figure 12. Velocity vectors for the Baseline case of and the BDSR case of the flat plate for different injection ratio at X/D = 3, M = 0.25, 0.5, 0.85, 1.0 and 1.5.

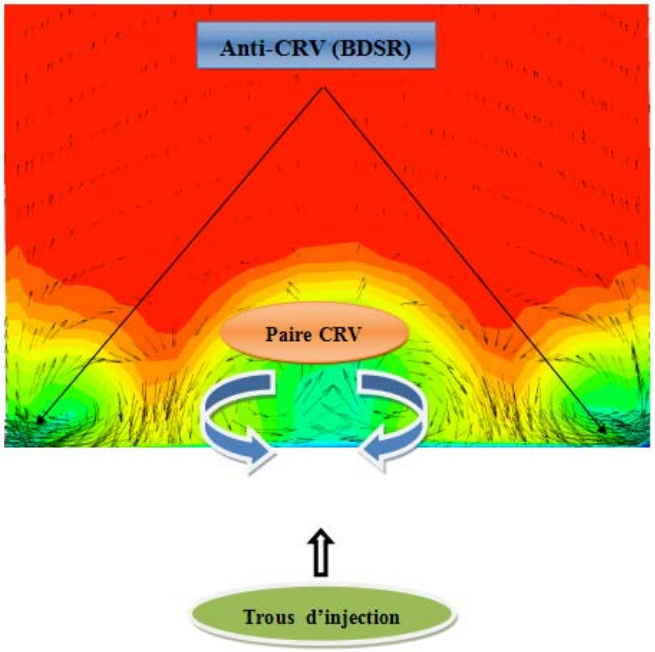

Figure 13. Schematic of velocity vector.

Figure 12 shows a comparison for velocity vectors for different injection ratios M = 0.25, M=0.5, M=0.85, M=1.0, M=1.5. On the X/D=3plan for the two configurations. In the case of Baseline, the presence of the CRV pair with a low density of velocity vectors at both sides of the plate in the lateral direction as shown by several studies [24, 25, 26]. In the case of BDSR, it is clear that the rotation directions of the vectors are opposite to those of the CRVs in the coolant jet stream, they are referred as anti-CRVs. These vectors are shown in Figure 13.Anti-CRV_s could countervail the detrimental effects of CRVs in the cooling jetstream. Consequently, the separation of the coolant jet stream from the surface of the plate will be postponed due to the existence of BDSR in comparison with the case of Baseline. The distance between the CRVs was found to be elongated in the lateral direction due to the existence of BDSR compared to Baseline case.

7. Conclusion

In this work, the concept of the Barchan-dune-shape ramp upstream of the injection hole has been numerically studied. The results were obtained by the computational simulation of film cooling through two configurations, with a comparison of injection ratio.

The first case is a Baseline configuration with a flat plate without geometry change. The second case is a BDSR configuration with a modification of the geometry. The results obtained show that the film cooling is better with BDSR case than with Baseline case. From The use of the BDSR upstream of the injection hole acts as an obstacle for the hot flow. This has a significant effect on the film cooling efficiency. Thus, the film cooling effectiveness is improved due to the additional anti-kidney vortex pair generated by the interaction between the mainstream and the Barchan-dune-shape ramp coolant. Which would help the coolant air to reattach on the flat plate, covering the whole surface by obtaining a better value of centerline and laterally film cooling effectiveness. According to the results obtained, we note that the most favorable rate for the two configurations is M=0.85.

Nomenclature

BDSR Barchan-dune-shaped-ramp
D film-cooling hole diameter
L spanwise dimension of the plate
l length of the injection hole
M Blowing ratio
T temperature
U velocity
CRVP/CRV Counter-rotating vortex pairs
x, y, z Cartesian coordinate

Greek

η	adiabatic film cooling effectiveness
$<\eta>$	laterally averaged adiabatic effectiveness
ρ	density

Subscripts

∞	Free-streamcondition
C	Coolant

References

[1] F. Ebacher. (2017). “Analyse du refroidissement par film de la paroi de bout de pales d’une turbine en céramique à configuration renversée” (Film cooling analysis of the blade end wall of an inverted ceramic turbine). *M.Sc. Theses*, 2017.

[2] Goldstein, R. J., Eckert, E. R. G., Eriksen, V. L., and Ramsey, J. W. (1970). “Film Cooling Following Injection Through Inclined Circular Tubes.” Israel Journal of Technology, Vol. 8, No. 1-2, pp. 145-154.

[3] Mehendale, A. B., Han, J. C., and Ou, S. (1991). “Influence of High Mainstream Turbulence on Leading Edge Heat Transfer.” ASME Journal of Heat Transfer, Vol. 113, November 1991, pp. 843-850.

[4] Honami, S., Shizawa, T., and Uchiyama, A. (1994). “Behavior of the Laterally Injected Jet in Film Cooling: Measurements of Surface Temperature and Velocity/Temperature Field Within the Jet.” ASME Journal of Turbomachinery, Vol. 116, pp. 106-112.

[5] Schmidt, D. L., Sen, B. (1996). “Film Cooling with Compound Angle Holes: Adiabatic Effectiveness.” ASME Journal of Turbomachinery, Vol. 118, pp. 807-813.

[6] Ligrani, P. M., Wigle, J. M., Ciriello, S., and Jackson, S. W. (1994). “Film-cooling From Holes with Compound Angle Orientations: Part 1- Results Downstream of Two Staggered Rows of Holes with 3d Spanwise Spacing.” ASME Journal of Heat Transfer, Vol. 116, No. 2, 1994, pp. 341-352.

[7] Ligrani, P. M., Wigle, J. M., and Jackson, S. W. (1994). “Film-cooling From Holes with Compound Angle Orientations: Part 2- Results Downstream of a Single Row of Holes with 6d Spanwise Spacing.” ASME Journal of Heat Transfer, Vol. 116, No. 2, 1994, pp. 353-362.

[8] Bunker, R. S. (2002). Film Cooling Effectiveness Due to Discrete Holes Within Transverse Surface Slots, Proceedings IGTI Turbo Expo, Amsterdam, The Netherlands, ASME Paper No.GT-2002-30178.

[9] S. Baheri and B. A. Jubran. (2012). The Effect of Turbulence Intensity on Film Cooling of Gas Turbine Blade from Trenched Shaped Holes. J. Heat & Mass Transfer, 05/2012, 48(5).

[10] Wang, T., Chintalapati, S., Bunker, R.S., and Lee, C. P. (2000). “Jet Mixing in a Slot.” Experimental Thermal and Fluid Science, Vol. 22, pp. 1-17.

[11] Lu, Y., Nasir, H., and Ekkad, S.V. (2005). “Film Cooling from a Row of Holes Embedded in Transverse Slots.” ASME Paper IGTI2005-68598.

[12] Kebir, F. and Azzi, A. (2018). Study of wave number effect in wavy plate for improving the film cooling effectiveness at spanwise direction. Numerical Heat Transfer, Part A: Applications, 73(6), 408-427.

[13] Ben Ali Kouchih, F., Boualem, K., Grine, M., and Azzi, A. (2020). The Effect of an Upstream Dune-Shaped Shells on Forward and Backward Injection Hole Film Cooling. Journal of Heat Transfer, 142(12), 122302.

[14] Gritsch, M., Schulz, A., and Wittig, S. (1998). “Heat Transfer Coefficient Measurements of Film Cooling Holes with Expanded Slots.” American Society of Mechanical Engineers, ASMEPaper 98-GT-28, June 1998.

[15] Gritsch, M., Schulz, A., and Wittig, S. (2016). “Adiabatic Wall Effectiveness Measurements of Film Cooling Holes with Expanded Exits.” ASME Journal of Turbomachinery, Vol. 120, No. 3, 1998, pp. 549-556. Han, C., Chi, Z., Ren, J., and Jiang, H. (2016). GT2013-94561. 1-11.

[16] Hassan, H. and Abdullah, K. (2017). Combined-hole film cooling with the application of double flow control devices. MATEC Web of Conferences, 135, 1-9.

[17] Wang, J., Tian, K., Luo, J., and Sundén, B. (2019). Effect of hole configurations on film cooling performance. Numerical Heat Transfer; Part A: Applications, 75(11), 725.

[18] Zaman, K., Rigby, D., and Heidmann, J. (2010). “Experimental Study of an Inclined Jet-in-Cross-Flow Interacting with a Vortex Generator.” AIAA Paper No. 2010-88.

[19] Shinn, A. F. and Vanka, S. P. (2013). “Large Eddy Simulations of Film-Cooling Flows with a Micro-Ramp Vortex Generator.” ASME J. Turbomach., 135(1), p. 011004.

[20] Zhou, W. and Hu, H. (2016). “Improvements of Film Cooling Effectiveness by Using Barchan Dune Shaped Ramps.” Int. J.

Heat Mass Transfer, 103, pp. 443-456.

[21] Zhou, W., and Hu, H. (2017). “A Novel Sand-Dune-Inspired Design for Improved Film Cooling Performance.” Int. J. Heat Mass Transfer, 110, pp. 908-920.

[22] Zhang, X. Z. and Hassan, I. (2006). Film cooling effectiveness for an advanced-louver cooling scheme for gas turbines. Journal of Thermophysics and Heat Transfer, 20(4), 754-763.

[23] T. F. Frict and A. Roshko. (1994). Vortical structure in the wake of a transverse jet. J Fluid Mech, pp. 1-47 (1994).

[24] Miloš Ilak, Philipp Schlatter, Shervin Bagheri, and Dan, S. (2012). Henningson, Bifurcation and stability analysis of a jet in crossflow: onset of global instability at a low velocity ratio, pp. 94-121, 2012.

[25] D. R. Getsinger, L. Gevorkyan, O. I. Smith, and A. R. Karagozian. (2014). Structural and stability characteristics of jets in crossflow. J. Fluid Mech., vol. 760, pp. 342-367, 2014.

[26] Sinha, D. Bogard and N. Crawford. (1991). Film Cooling Effectiveness Downstream of a Single Row of Holes with Variable Density Ratio. J. Turbomach., vol. 113, pp. 442-449, 1991.